doi:10.1093/brain/awm276 *Brain* (2008), **131**, 109–119

Changes in readthrough acetylcholinesterase expression modulate amyloid-beta pathology

Amit Berson,[1] Marlen Knobloch,[2] Mor Hanan,[1] Sophia Diamant,[1] Michal Sharoni,[1] Daniel Schuppli,[2] Brian C. Geyer,[3] Rivka Ravid,[4] Tsafrir S. Mor,[3] Roger M. Nitsch[2] and Hermona Soreq[1]

[1]The Eric Roland Center for Neurodegenerative Diseases, Institute of Life Sciences, The Hebrew University of Jerusalem, 91904 Jerusalem, Israel, [2]Division of Psychiatric Research, University of Zurich, 8008 Zurich, Switzerland, [3]School of Life Sciences, Biodesign Institute, 87450I, Arizona State University, Tempe, AZ 85287-450I, USA and [4]Netherlands Brain Bank, 1105 AZ Amsterdam, The Netherlands

Correspondence to: Hermona Soreq, Israel Center of Neuronal computation (ICNC), Safra Campus, Givat Ram, Jerusalem, 91904, Israel
E-mail: soreq@cc.huji.ac.il

Alzheimer's disease has long been known to involve cholinergic deficits, but the linkage between cholinergic gene expression and the Alzheimer's disease amyloid pathology has remained incompletely understood. One known link involves synaptic acetylcholinesterase (AChE-S), shown to accelerate amyloid fibrils formation. Here, we report that the 'Readthrough' AChE-R splice variant, which differs from AChE-S in its 26 C-terminal residues, inversely exerts neuroprotective effects from amyloid β (Aβ) induced toxicity. *In vitro*, highly purified AChE-R dose-dependently suppressed the formation of insoluble Aβ oligomers and fibrils and abolished Aβ toxicity to cultured cells, competing with the prevalent AChE-S protein which facilitates these processes. *In vivo*, double transgenic APPsw/AChE-R mice showed lower plaque burden, fewer reactive astrocytes and less dendritic damage than single APPsw mice, inverse to reported acceleration of these features in double APPsw/AChE-S mice. In hippocampi from Alzheimer's disease patients ($n = 10$), dentate gyrus neurons showed significantly elevated AChE-R mRNA and reduced AChE-S mRNA. However, immunoblot analyses revealed drastic reductions in the levels of intact AChE-R protein, suggesting that its selective loss in the Alzheimer's disease brain exacerbates the Aβ-induced damages and revealing a previously unforeseen linkage between cholinergic and amyloidogenic events.

Keywords: Alzheimer's disease; acetylcholinesterase; alternative splicing; β-Amyloid

Abbreviations: Aβ = amyloid-β; ACh = acetylcholine; AChE = acetylcholinesterase; BChE = butyrylcholinesterase; DG = dentate gyrus; FISH = Fluorescent *in situ* hybridization; LS = low salt; LSD = low salt detergent; NDC = non-demented control; RT = reverse transcriptase

Received June 13, 2007. Revised September 5, 2007. Accepted October 22, 2007. Advance Access publication December 3, 2007

Introduction

Alzheimer's disease has been identified as a cholinergic deficit in the early eighties (Coyle *et al.*, 1983), which led to the development of cholinesterase inhibitors as the leading currently used Alzheimer's disease drugs (Lleo *et al.*, 2006). The cognitive symptoms in Alzheimer's disease involve learning and memory deficits accompanied by neuropsychiatric disturbances, considered to be partially induced by the loss of cholinergic neurons (Cummings and Back, 1998). These neurons notably express the acetylcholine (ACh) hydrolysing enzyme acetylcholinesterase (AChE) (Landwehrmeyer *et al.*, 1993). The presence of AChE in the amyloid plaques characteristic of Alzheimer's disease brains (Carson *et al.*, 1991), the non-catalytic enhancement of amyloid-β (Aβ) fibrils formation by the major 'Synaptic' AChE variant [AChE-S, also called AChE-T; (Massoulie, 2002)] (Inestrosa *et al.*, 1996) and its suppression by the highly homologous enzyme butyrylcholinesterase [BChE; (Diamant *et al.*, 2006)], renewed the interest in both ACh and cholinesterases as potential modulators of the Alzheimer's disease neuropathology. Supporting this notion, muscarinic agonists attenuate both Aβ and tau pathologies and delay the development of cognitive impairments in transgenic mice (Caccamo *et al.*, 2006).

However, that the brain's ACh hydrolysing activity decreases relatively late in the Alzheimer's disease process, raised doubts regarding the causal involvement of AChE in Alzheimer's disease (Davis *et al.*, 1999). Importantly, AChE is not one but several proteins, because alternative splicing and alternate promoter usage generate various forms of AChE, differing in their N- and C-termini (Meshorer and Soreq, 2006) but all capable of hydrolysing ACh. For comparison, splice variants of other genes often show inverse properties [e.g. pro-apoptotic, or anti-apoptotic features of splice variants of Bcl2 (Shin and Manley, 2004)]. This raised the possibility that distinct AChE variants exert various effects on the Alzheimer's disease process.

Currently available studies on the involvement of AChE in Alzheimer's disease largely reflect the properties and expression patterns of the tetramer-forming AChE-S, the prominent variant in the mammalian brain (Soreq *et al.*, 1990; Ben Aziz-Aloya *et al.*, 1993). AChE-S was shown to enhance Aβ fibrils formation *in vitro* (Inestrosa *et al.*, 1996), enhance their neurotoxic effects *ex vivo* (Alvarez *et al.*, 1998) and facilitate Alzheimer's disease plaque formation *in vivo* (Rees *et al.*, 2005). However, aging involves a gradual increase in the blood levels of the monomeric, soluble, stress-induced AChE-R variant (Sklan *et al.*, 2004), which differs from AChE-S in its 26 C-terminal amino acid residues. AChE-R accumulates following swim stress (Kaufer *et al.*, 1998), head injury, immobilization stress or exposure to cholinesterase inhibitors (Meshorer and Soreq, 2006). Since transgenic overexpression of AChE-R attenuates aging and stress-associated neuropathologies, unlike AChE-S which enhances these features (Sternfeld *et al.*, 2000), we specifically addressed the role of AChE-R in Alzheimer's disease progression. AChE-R effects were examined on Aβ fibril formation *in vitro*, on Aβ toxicity to cultured cells *ex vivo* and on amyloid plaque formation and neurotoxicity in double-transgenic mice *in vivo*. Finally, ACHE gene expression and protein levels were monitored in hippocampus samples of human Alzheimer's disease patients as compared with non-demented controls (NDCs).

Materials and methods

Human brain tissue

Brain tissue from Alzheimer's disease patients ($n = 10$) and NDCs ($n = 5$) was provided by the Netherlands Brain Bank. Ethical approval and written informed consent from the donors or the next of kin was obtained in all cases. Neuropathological Braak staging of neurofibrillary changes (I–VI) was performed *post-mortem* (Braak and Braak, 1991). Individual case details are described in Table 1.

Transgenic mice

AChE-R overexpressing mice (FVB/N background) (Pick *et al.*, 2006) were crossed with mice transgenic for human APP-695 with the 'Swedish' mutation (Hsiao *et al.*, 1996) (B6/SJL background) to generate double-transgenic APPsw/AChE-R mice. Backcrossing to B6/SJL wild-type generated single and double transgenic mice. Genotyping involved tail tip PCR. Seventy-five-week-old mice [APPsw ($n = 5$) and AChE-R/APPsw ($n = 5$)] were anaesthetized and perfused with ice-cold phosphate-buffered saline (PBS). One hemisphere was postfixed overnight at 4°C in 4% paraformaldehyde, washed with PBS and paraffin embedded. The other was dissected and stored at −80°C until protein extraction. Animal experiments were approved by the veterinary service of the Department of Animal Health, University of Zurich.

Immuno-blots

Human samples

Immuno-blot analysis of human hippocampal homogenate samples involved rabbit anti-human AChE-R antibodies directed at the unique C-terminus of AChE-R (1:700) (Sternfeld *et al.*, 2000), anti total AChE (H134, Santa Cruz, Santa Cruz, CA, 1:700) and anti α-tubulin (Santa Cruz, 1:2000).

Mouse samples

For insoluble Aβ measurements, detergent-insoluble pellets were resolved in 70% FA and neutralized with 10 M NaOH. Extracts were separated by 8 M urea gel, blotted onto PVDF membrane, boiled for 5 min in PBS and blocked in TBS containing 4% milk for 1 h at room temperature. Membranes were incubated overnight with the 6E10 antibody at 4°C and visualized by an anti-mouse peroxidase-conjugated antibody (Jackson, West grove, PA) and ECL reactions. SDS–PAGE and immuno-blot of low-salt detergent (LSD) fraction with the 6E10 antibody was used for amyloid-precursor protein (APP) analysis.

RNA procedures

Fresh frozen human hippocampi were coronally cut. RNA was extracted (RNeasy lipid tissue kit, Qiagen, Valencia, CA), DNase treated and its integrity confirmed by gel electrophoresis. cDNA synthesis (Promega, Madison, WI) involved 0.4 μg RNA samples in 20 μl reactions. Duplicate real-time reverse transcriptase (RT)–PCR tests involved ABI prism 7900HT, SYBR green master mix (Applied biosystems, Foster City, CA) and ROX, a passive reference dye for signal normalization across the plate. Primer

Table 1 Patient details

Patient (gender; age)	Diagnosis (PMD)
02-005 (f;42)	AD, Braak 6 (06:10)
02-079 (f;58)	AD, Braak stage unavailable (04:30)
02-056 (f;85)	AD, Braak 5 (03:45)
02-061 (f;76)	AD, Braak 5 (10:45)
02-080 (f;86)	AD, Braak 5 (04:10)
02-085 (f;79)	AD, Braak 5 (04:15)
02-088 (f;78)	AD, Braak 5 (04:00)
02-099 (m;69)	AD, Braak 6 (05:30)
02-102 (f;88)	AD, Braak 5 (03:15)
03-009 (m;65)	AD, Braak 5 (07:20)
99-067 (f;59)	NDC, AD, Braak 1 (06:20)
00-017 (f;72)	NDC, AD, Braak 1 (06:45)
00-025 (f;41)	NDC, AD, Braak 0 (13:30)
01-021 (m;82)	NDC, AD, Braak 1 (07:40)
01-046 (m;88)	NDC, AD, Braak 1 (07:25)

Patient numbers, gender, age, Braak stage and *post-mortem* delay (PMD) in hours are shown. NDC = non-demented control.

sequences are listed in Table 2. Reference transcript of 18S rRNA was used. Annealing temperature was 60°C for all primers. Serial dilution of samples served to evaluate primers efficiency and the appropriate cDNA concentration that yields linear changes. Melting curve analysis and amplicons sequencing verified the identity of end products. For absolute quantification, a calibration curve was constructed using AChE-S and AChE-R specific plasmids.

Fluorescent *in situ* hybridization (FISH)

De-paraffinization of hippocampal coronal 7 μm paraffin sections involved two washes in xylene, then in 100%, 75%, 50% and 25% ethanol in PBT (0.13 M NaCl, 7 mM $Na_2HPO_4{\cdot}7H_2O$, 3 mM $NaH_2PO_4{\cdot}H2O$, 0.1% Tween-20), and finally twice with PBT. Quenching was applied to suppress autofluorescence (Sun *et al.*, 2002). Sections were then treated with10 μg/ml proteinase K (Boehringer Mannheim, Mannheim, Germany) for 8 min and washed with PBT. Prehybridization in 50% formamide, 5 × Sodium saline citrate (SSC), 50 μg/ml yeast tRNA (Boehringer Mannheim) and 50 μg/ml heparin (Sigma, Jerusalem, Israel) in DDW was at 60°C for 30 min. Pre-heated hybridization mix (including biotin-conjugated probes, 10 μg/ml) was added (in a humid chamber, 90 min or overnight at 52°C for the AChE-S and AChE-R probes, respectively). Two high-stringency washes at 60°C in solutions 1 (50% formamide, 5× SSC pH 4.5, 0.5% sodium dodecyl sulphate in DDW), and 2 (50% formamide, 5× SSC pH 4.5 in DDW) were followed by two washes in TBST (25 mM Tris–HCl pH 7.5, 136 mM NaCl, 2.7 mM KCl, 0.05% Tween-20) and incubation with 1% skimmed milk in TBST to prevent non-specific streptavidin interactions. Detection involved 40 min incubation with streptavidin-conjugated Cy3 (Jackson) diluted 1:100, at room temperature. Slides were then washed three times with TBST, once in DDW, and mounted with ImmunoMount (Shandon, Pittsburgh, PA). All slides were handled simultaneously to minimize inter-slides variability. Negative control slides were incubated with a zeta-globin probe that is not expressed in the adult brain. The 2′*O*-methyl, 5′-Biotinylated cRNA probes (Microsynth, Balgach, Switzerland) used in this study are detailed in Table 3.

Table 2 FISH probes

Probe	Accession no	Sequence 5′–3′	Position
hAChE-S	NM.000665	ccgggggacgucgggguggg gugggggaugggcagaguc uggggcucgucu	2022–2071
hAChE-R	L42812	cuagggggagaagagaggggu uacacuggcgggcucccac uccccuccuc	3188–3238
hZeta-globin	BC027892	tgatggtcctctcagtcttggtc agagacatggcggcagggtg ggcagct	17–66

Protein fractionation and AChE activity tests

Low-salt (LS) and LSD fractions of hippocampal homogenates were prepared as described (Gilboa-Geffen *et al.*, 2007). AChE catalytic activity was measured by an adaptation of a spectrophotometric method (Ellman *et al.*, 1961) to a micro titre plate assay.

Immunohistochemistry

Paraffin slices handled simultaneously to minimize inter-slides variability were deparaffinized and blocked for 1 h in Tris 10% serum-blocking solution. Primary antibodies were diluted in the blocking buffer and applied for 2 h, room temperature or overnight at 4°C: Anti Aβ, 6E10, 1:400 (Signet, Dedham, MA); Anti glial fibrillary acidic protein (anti GFAP, Sigma), 1:50; Anti microtubule-associated protein 2 (MAP2), 1:100 (Lab Vision, Fremont, CA). Corresponding biotin-conjugated secondary antibodies were used. 6E10 detection was with the ABC kit (Vector, Burlingame, CA) with 3,3′-diaminobenzidine as substrate. For anti-MAP2 and anti-GFAP, detection involved streptavidin-conjugated Cy3 (1:100, Jackson).

Zeiss (Oberhochen, Germany) Axioplan or Bio-Rad (Hemel Hempsted Hers, UK) MRC- 1024 confocal microscopy served for analysis. Labelling intensity was quantified with ImagePro Plus 4.5 (Media Cybernetics, Silver Spring, MD).

Cell culture and toxicity measurements

SH-SY5Y human neuroblastoma cells were cultured in a 1:1 mixture of Eagle's minimum essential medium and F12 medium (Sigma), containing 10% FCS and a mixture of 1% penicillin–streptomycin–amphotericin (Biological industries, Beit Haemek, Israel). Cells were plated in 48 well plates at $2{\cdot}10^5$ cells/well at 37°C in a humid 5% CO2 incubator. Synthetic Aβ (1-40) peptide (Sigma) was dissolved in dimethyl sulphoxide (DMSO) at 5 mM. To initiate partial fibrils formation Aβ was diluted to 100 μM in PBS and incubated alone or with recombinant human AChE-R from transgenic *Nicotiana benthamiana* plants (Geyer *et al.*, 2005) at a 1:100 ratio (1 μM AChE-R), for 24 h at 37°C. Aβ mixtures diluted 1:10 in low-serum medium yielding final concentrations of 10 μM Aβ and 0.1 μM AChE-R were applied to the cells for 3 days. Lactate dehydrogenase (LDH) activity (Diamant *et al.*, 1995) in the medium and cell counts served to asses cellular viability.

Aβ fibrils formation

For *in vitro* fibrils formation, synthetic Aβ (1-40 or 1-42) peptides (Sigma) dissolved in DMSO at 1.6 mM were sonicated (3 × 5 s

Table 3 Real-time RT–PCR primers

Isoform	Accession no	Forward primer 5′–3′	Position	Reverse primer 5′–3′	Position
hAChE-S	NM.000665	cttcctccccaaattgctc	1789–1807	tcctgcttgctgtagtggtc	1901–1920
hAChE-R	AY750146	cttcctccccaaattgctc	7092–7110	ggggagaagagaggggttac	7177–7196
HI8S rRNA	MI0098	cgccgctagaggtgaaattc	1049–1068	ttggcaaatgctttcgctc	1092–1110

pulses), filtered through 0.22 μm filters and stored in aliquots at −70°C (Klug *et al.*, 2003). The fluorescence signal of thioflavin T (ThT) (Sigma), a benzothiazole dye the excitation spectrum of which shifts from 340 to 450 nm when interacting with β-sheet amyloid structures, reflected the amount of amyloid fibrils formed (LeVine, 1993). Aliquots of 20 μl Aβ were diluted from the stock DMSO solution to a final concentration of 162 μM in PBS containing 0.02% Na-Azid using 96 wells plates (Nunc, Roskilde, Denmark). Following incubation (room temperature, 20 min), 80 μl of 1.25 μM ThT in 50 mM glycine buffer, pH 8.5, was added for 6 to 10 h shaking at 200 r.p.m. and 30°C. Water-dissolved recombinant AChE variants were added to yield the indicated molar ratio. Recombinant human AChE-S was produced in and purified from cultured HEK293 cells (Sigma). Fluorescence was measured at 10 min intervals, using a Spectro-fluorometer (Tecan, Maennedorf, Switzerland), with 450 nm excitation and 485 nm emission wavelengths (Diamant *et al.*, 2006).

Cross-linking

To specifically detect the effect of AChE-R on Aβ oligomeric forms, Aβ was incubated either with or without AChE-R (as above). At different time points, aliquots were separated to soluble and insoluble fractions by centrifugation. Photo-induced cross-linking of unmodified proteins [PICUP, (Fancy and Kodadek, 1999)] with ruthenium(II) Tris–bipyridyl dication [$Ru(II)bpy_3^{2+}$] was then used to identify the different oligomeric forms of Aβ present in the supernatant fraction. The insoluble pellet was resuspended in 8 M urea and diluted to 4 M. SDS–PAGE on 10–20% Tris–tricine gels of these samples was followed by silver staining.

Statistical analyses

All pair-wise comparisons involved the non-parametric Mann–Whitney significance test. Correlation significance was analysed with Pearson's and Spearman's tests.

Results

AChE-R attenuates whereas AChE-S facilitates Aβ fibrils formation *in vitro*

To examine the specific contribution of different AChE splice variants to amyloid fibrils formation, we studied the *in vitro* aggregation behaviour of Aβ1-40 or Aβ1-42 in the presence of highly purified recombinant AChE-R (Geyer *et al.*, 2005; Evron *et al.*, 2007) as compared with recombinant AChE-S (Fig. 1A). Incubation of AChE-S with Aβ1-40, at the range of 1:1000–1:1600 ratio, predictably shortened the lag period preceding fibril formation and accelerated the rate of ThT incorporation into Aβ fibrils, supporting previous reports of a direct involvement of AChE-S with the progression of this process (Inestrosa *et al.*, 1996) (Fig. 1B). In contrast, recombinant AChE-R in 1:400–1:1600 ratios to Aβ impeded Aβ fibril formation for up to 1100 min (Fig. 1C). The observed changes involved prolonged lag time and reduced rate of fibrils formation (Fig. 1C), inversely to the facilitation effect of AChE-S. The effects of AChE-R and AChE-S were dose dependent and their presence in the reaction changed the final yield of fibrils formed (Fig. 1B and C). Since the major amyloidogenic Aβ form is the 1-42 amino acids peptide, we repeated the ThT assay with Aβ1-42 and found similar effects (Fig. 1D and E), suggesting that AChE variants will effect the oligomerization of both Aβ variants *in vivo*. Since both AChE-S and AChE-R are expressed in the human brain it was interesting to test the simultaneous effect of both variants. At five different molar ratios between AChE-S and AChE-R (1:1, 1:2, 2:1, 1:5 and 5:1), AChE-R exhibited a dominant inhibitory effect over AChE-S (Fig. 1F). Because AChE-S and AChE-R differ in their C-terminal domain, we predicted that this region may be at least partially responsible for the marked differences observed. We therefore pre-incubated AChE-R with a specific antibody against its unique C-terminus and found that masking this region abolished AChE-R's ability to inhibit fibrils formation (Fig. 1G). Interestingly, while the pre-incubated AChE-R–antibody complex did not affect the reaction rate or the final fibrils yield, it prolonged the lag phase, suggesting that other domains (e.g. the peripheral active site) may also be involved (Fig. 1G).

Different oligomeric forms of Aβ vary in their effects on neuronal toxicity and learning and memory (Ross and Poirier, 2004; Lesne *et al.*, 2006). Therefore, it was important to examine the specific stage of fibrils formation with which AChE-R interferes. To this end, we incubated Aβ1-40 with or without recombinant AChE-R, separated the soluble from insoluble fractions and analysed the kinetics of Aβ oligomerization. First, the soluble fraction was subjected to photo-induced cross-linking followed by SDS–PAGE and silver staining. This analysis revealed three distinct time frames in which AChE-R affects Aβ oligomerization differentially (Fig. 2A). For the first 5 h of incubation, Aβ dimers, tetramers and pentamers were produced with or without AChE-R. However, between the sixth and seventh hours of incubation, most of the light Aβ forms (up to 20 kDa, corresponding to Aβ pentamers) disappeared from the soluble samples including Aβ alone, yet were still clearly present when Aβ was incubated with AChE-R. After 20 h of incubation, no soluble oligomeric forms of Aβ were found regardless of the presence of AChE-R (Fig. 2A). This reflected the generation of insoluble fibrils, which became apparent from SDS–PAGE of the insoluble Aβ aggregates, resuspended in 8 M urea. Thus, after 6 and 7 h of incubation, the samples containing AChE-R included considerably less insoluble Aβ than those without it (Fig. 2B). By 20 h of incubation, no differences were found between the insoluble fractions with Aβ alone and with AChE-R, indicating that AChE-R delayed but did not completely inhibit the formation of heavy Aβ oligomers. Interestingly, after 20 h of incubation, intact AChE-R largely shifted from the soluble fraction (Fig. 2A) into the insoluble fraction (Fig. 2B), indicating its direct contact with the amyloid fibrils.

In addition to the full-length recombinant AChE-R, two shorter peptides are also detectable by silver staining.

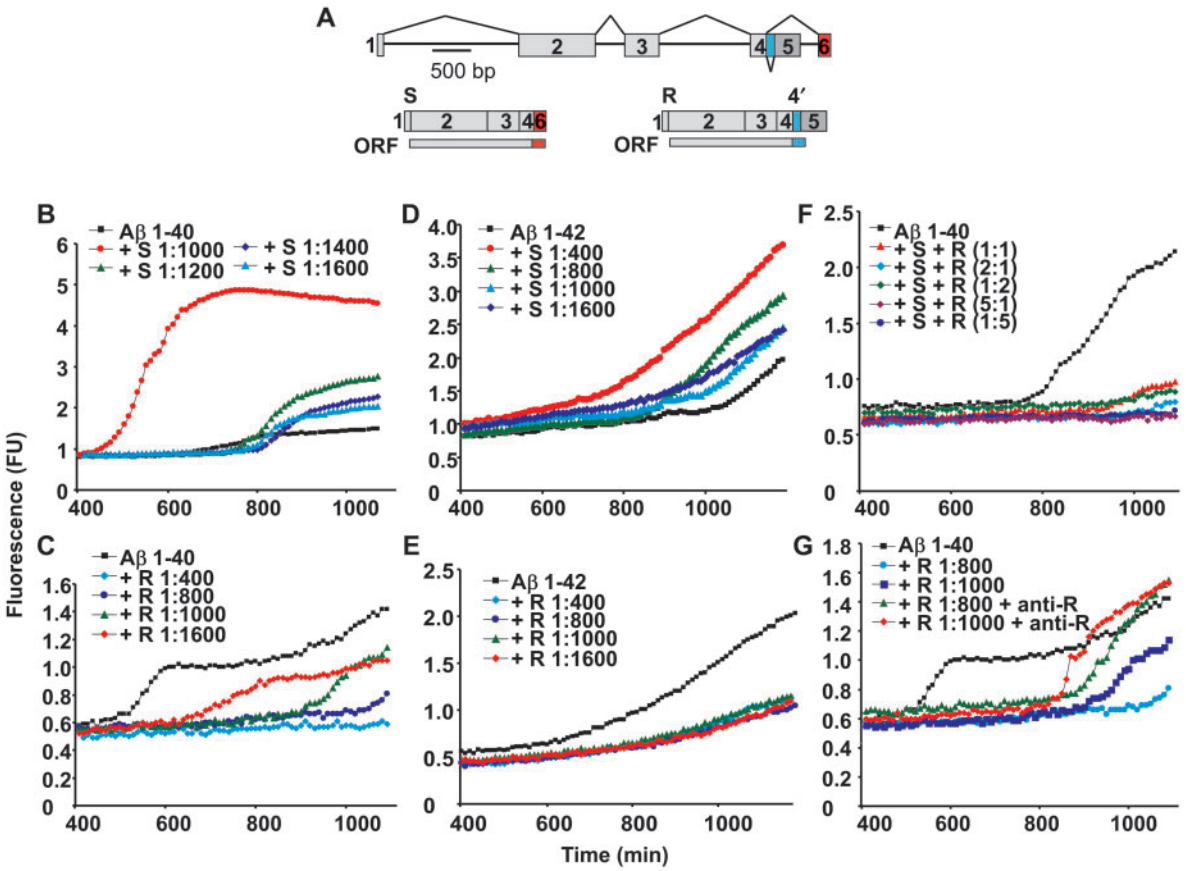

Fig. 1 AChE-R attenuates while AChE-S facilitates Aβ fibrils formation *in vitro*. (**A**) Scheme: AChE-S and AChE-R are produced from alternatively spliced transcripts of the single *ACHE* gene. Exons 2, 3 and 4 (light grey) encode the common core of these variants. AChE-R mRNA includes pseudo-intron 4 (4′) and exon 5, whereas AChE-S mRNA includes exon 6. Their protein products deviate in their C-terminal domains. Kinetics of Aβ fibrils formation was monitored using thioflavin T (ThT) fluorescence over time. (**B**) Shown is dose dependent effect of recombinant AChE-S protein on Aβ1-40 fibrils formation. (**C**) Dose-dependent effect of recombinant AChE-R protein on Aβ1-40 fibrils formation. (**D**) Dose-dependent effect of recombinant AChE-S protein on Aβ1-42 fibrils formation. (**E**) Dose-dependent effect of recombinant AChE-R protein on Aβ1-42 fibrils formation. (**F**) Simultaneous presence of both AChE-S and AChE-R at different molar ratios. Note a dominant effect of AChE-R over AChE-S, resulting in inhibition of Aβ1–40 fibrils formation. (**G**) Pre-incubation of AChE-R with a specific antibody directed to the C-terminal domain (anti-R) results in loss of inhibitory effect.

Immuno-blot analysis using an antibody directed to the unique C-terminus of AChE-R confirmed the identity of these bands as an extended C-terminal AChE-R fragments (Fig. 2A). Importantly, unlike intact AChE-R, these peptides did not shift from the soluble fraction into the insoluble fraction, suggesting that interaction with the fibrils requires intact AChE-R. Together, these analyses suggested that AChE-R production might serve to attenuate amyloid fibrils formation and called for challenging this prediction in an *in vivo* context.

AChE-R reduces plaque burden in double transgenic APPsw/AChE-R mice

To test the ability of AChE-R to attenuate amyloid fibrils assembly *in vivo*, we generated double-transgenic APPsw/AChE-R mice by mating APPsw mice (Hsiao *et al.*, 1996) with AChE-R overexpressing ones (Pick *et al.*, 2006) and comparing their cortical plaque burden with that of single transgenic APPsw mice. First, we wished to verify that AChE-R levels are selectively higher in APPsw/AChE-R mice as compared with the APPsw single transgenics. Therefore, we fractionated hippocampal homogenates to a LS fraction, enriched with soluble AChE-R and a LSD fraction, enriched with membrane-anchored AChE-S. Predictably, AChE-R but not AChE-S activity was higher in APPsw/AChE-R mice (Fig. 3A and B). Nevertheless, APPsw and APPsw/AChE-R mice showed similar summed total AChE activity (364 ± 57 and 318 ± 105 nmol/min mg, respectively), suggesting that the overall cholinergic balance is maintained in these animals. Immuno-blot analysis further validated that AChE-R overexpression did not change APP levels in hippocampal homogenates (Fig. 3C). Compatible with our *in vitro* results, APPsw/AChE-R mice showed considerably lower cortical Aβ plaque burden than parent strain APPsw mice, as demonstrated by labelling with the 6E10 anti Aβ antibody, Congo red and thioflavin-*S* stainings (Fig. 3D and E, $P < 0.05$, Mann–Whitney test in

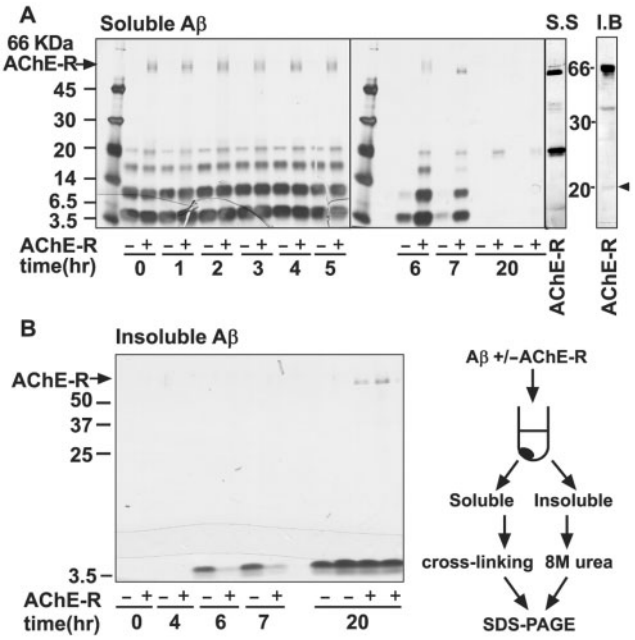

Fig. 2 Kinetics of AChE-R's effect on Aβ oligomerizarion. Silver staining of soluble (**A**) and insoluble (**B**) Aβ samples incubated for the indicated times with or without AChE-R. Note the difference in soluble oligomeric and insoluble forms after 6 and 7 h of incubation. Right insets: Silver staining (S.S) of recombinant AChE-R reveals two bands, one of which with similar MW to Aβ tetramers. A similar size band is also detectable by immuno-blot (I.B) with an anti-AChE-R antibody. Note a different scale for S.S and I.B. Scheme: the experimental outline.

all labelling paradigms). Moreover, immuno-blotting of SDS-insoluble pellets demonstrated lower levels of insoluble Aβ in hippocampal homogenates of APPsw/AChE-R mice (Fig. 3F). This phenotype was a mirror image of that we previously observed in APPsw/AChE-S mice (Rees *et al.*, 2005), substantiating our working hypothesis that these two AChE isoforms, which only differ in their C-terminal peptides (Meshorer and Soreq, 2006), exert inverse *in vivo* effects on Aβ fibrils formation both *in vitro* and in the mouse brain.

AChE-R exerts *in vivo* and *ex vivo* neuroprotection from Aβ toxicity

We next examined whether the reduction in Aβ plaque burden in APPsw/AChE-R mice reflected decreased neurotoxicity. The density of reactive astrocytes surrounding Aβ plaques, an indicator of the inflammatory reaction (Matsuoka *et al.*, 2001), was quantified by assessing GFAP labelling. Fewer reactive astrocytes appeared in the vicinity of Aβ plaques in the frontal cortex of double-transgenic APPsw/AChE-R mice compared to their single-transgenic littermates (Fig. 4A and B, $P<0.05$). Since Aβ plaques were shown to associate with dendritic abnormalities (Tsai *et al.*, 2004), we further immunolabelled the microtubule-associated protein MAP2 as a marker of dendritic integrity. Single-transgenic APPsw mice showed reduced immunoreactivity of frontal cortex MAP2, an effect which was

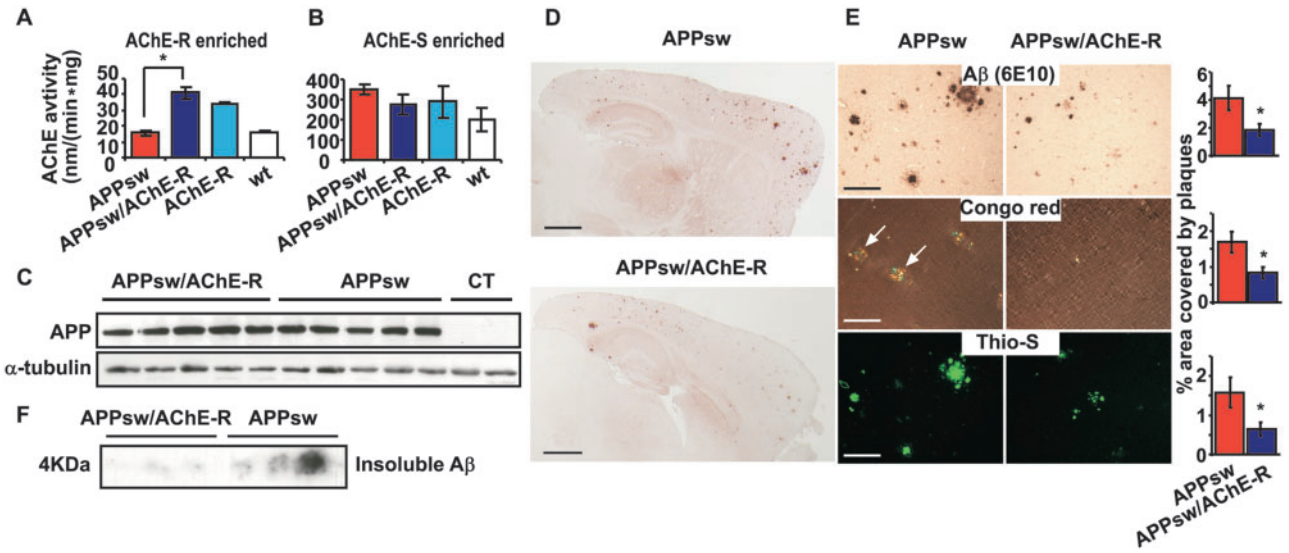

Fig. 3 AChE-R ameliorates Aβ burden in double-transgenic APPsw/AChE-R mice. (**A, B**) Hydrolytic AChE activities in APPsw/AChE-R hippocampi. Hippocampal AChE activities in transgenic brains were measured in low salt fraction, enriched with soluble AChE-R (**A**) and low-salt detergent fraction, enriched with membrane-anchored AChE-S (**B**). AChE-R activity is ~3-fold higher in APPsw/AChE-R mice compared with APPsw transgenics ($^*P<0.01$, Mann–Whitney test). (**C**) APP levels are not changed in APPsw/AChE-R. Immuno-blot analysis of APPsw/AChE-R and APPsw hippocampal samples using the 6E10 antibody. (**D, E**) Aβ plaque burden was assessed by labelling sections from single transgenic APPsw and double-transgenic APPsw/AChE-R mice with the 6E10 antibody, congo red and thioflavin-S. (**D**) Low magnification 6E10 immunoreactivity images of APPsw and APPsw/AChE-R mice. Scale bar = 1 mm (**E**) Representative enlarged fields from the frontal cortex. Quantification graphs show area covered with plaques (% ± SEM). APPsw $n=5$, APPsw/AChE-R $n=5$. Scale bar = 200 μm. ($^*P<0.05$, Mann–Whitney test). (**F**) Insoluble Aβ levels are reduced in APPsw/AChE-R mice. Immuno-blot analysis of SDS-insoluble hippocampal samples with an 8 M urea SDS–PAGE.

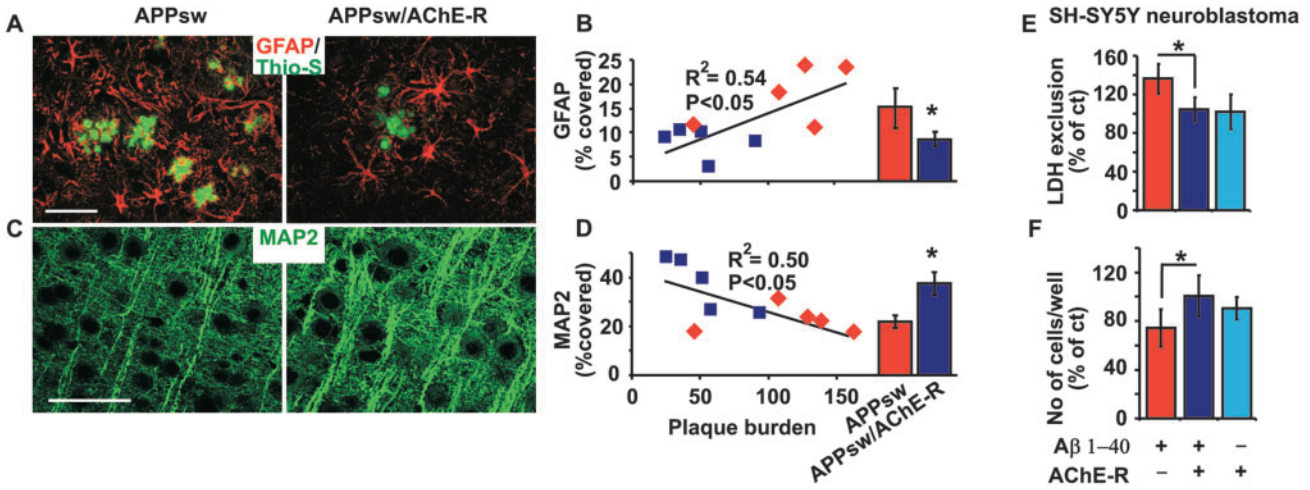

Fig. 4 AChE-R reduces Aβ toxicity *in vivo* and *ex vivo*. (**A**) GFAP astrocytic labelling (red) around β-amyloid plaques (green) in frontal cortices of APPsw and APPsw/AChE-R mice. Scale bar = 50 μm. (**B**) GFAP staining (percentage area covered ± SEM) and correlation to Aβ plaque burden. APPsw $n = 5$, APPsw/AChE-R $n = 5$. (*$P < 0.05$, Mann–Whitney test, $P < 0.05$, Pearson test for correlation). (**C**) MAP2 labelling in APPsw and APPsw/AChE-R frontal cortices. Scale bar = 50 μm. (**D**) MAP2 staining (percentage area covered ± SEM) and correlation to Aβ plaque burden. APPsw $n = 5$, APPsw/AChE-R $n = 5$. (*$P < 0.05$, Mann–Whitney test. $P < 0.05$, Pearson test for correlation). (**E**) LDH exclusion test of human neuroblastoma SH-SY5Y cells incubated with 10 μM Aβ 1-40 alone or with 1:100 recombinant AChE-R for 3 days. Note that AChE-R restores medium LDH activity to that of the control, while having no effect on its own. $n = 8$, One of two reproducible experiments. Error bars ± SD. (**F**) SH-SY5Y cell counts after treatment with 10 μM Aβ 1-40 alone or with 1:100 recombinant AChE-R for 3 days. Note that AChE-R restores full cell survival in the presence of Aβ 1-40. $n = 8$, One of two reproducible experiments. Error bars ± SD.

ameliorated in double-transgenic APPsw/AChE-R mice (Fig. 4C and D, $P < 0.05$). Importantly, GFAP labelling was significantly and positively correlated with plaque burden, whereas MAP2 labelling was inversely correlated with this hallmark (Fig. 4B and D, $P < 0.05$). This bimodal association validated the use of GFAP and MAP2 as biomarkers, suggesting that AChE-R overexpression actively delayed the Aβ-induced damages in the frontal cortex for over 75 weeks of age.

To yet more directly challenge the hypothesis that AChE-R suppresses Aβ neurotoxicity, synthetic Aβ1-40 was pre-incubated with or without recombinant human AChE-R, at a 1:100 ratio (AChE-R:Aβ), and mixtures were applied to cultures of SH-SY5Y neuroblastoma cells. Aβ, but not AChE-R increased lactate dehydrogenase (LDH) exclusion and decreased surviving cell counts (Fig. 4E and F). Importantly, when added to Aβ, AChE-R attenuated its toxic effects, sustaining control LDH exclusion values and cell survival as compared with Aβ effects (Fig. 4E and F).

Alzheimer's disease patient hippocampi show increased AChE-R mRNA but reduced AChE-R protein levels

The finding that AChE-R promotes neuroprotection against Aβ-induced damages called for testing if the mRNA expression and/or levels of this protein change in the Alzheimer's disease brain. We therefore examined the expression levels of AChE variants in human hippocampal tissues from Alzheimer's disease patients and NDCs. First, we explored AChE expression at the mRNA level using real-time RT–PCR and FISH on hippocampal homogenates and paraffin sections. RT–PCR analysis showed that AChE-R mRNA constitutes ~7% of AChE-S mRNA levels in the hippocampus of NDCs (51921 ± 14312 and 3781 ± 686 copies/ng total RNA, respectively), close to the 1:20 ratio we previously observed in newborn brain by cDNA screening (Ben Aziz-Aloya *et al.*, 1993). Importantly, we found an ~3-fold decrease in the level of the AChE-S mRNA variant ($P < 0.05$) which was accompanied by unchanged AChE-R mRNA levels in AD as compared with NDC hippocampi (Fig. 5A and B). Because RNA extracted from these tissue samples reflects a variety of hippocampal cell types, we further used variant-specific cRNA probes to label AChE variant mRNAs in hippocampal neurons. Given that different probes have unique hybridization characteristics, labelling intensity could only be compared between samples labelled with a specific probe. Extending the RT–PCR results, dentate gyrus (DG) neurons of Alzheimer's disease patients revealed significantly reduced AChE-S mRNA levels (Fig. 5C and D, $P < 0.05$). However, unlike the RT–PCR tests, the FISH analysis detected a significant increase in AChE-R mRNA within DG neurons of Alzheimer's disease patients (Fig. 5C and D, $P < 0.05$) as compared with its levels in NDCs. Similar effects were also observed in CA1 neurons (data not shown). Thus, AD hippocampal neurons produce less AChE-S mRNA but more AChE-R mRNA as compared with matched controls.

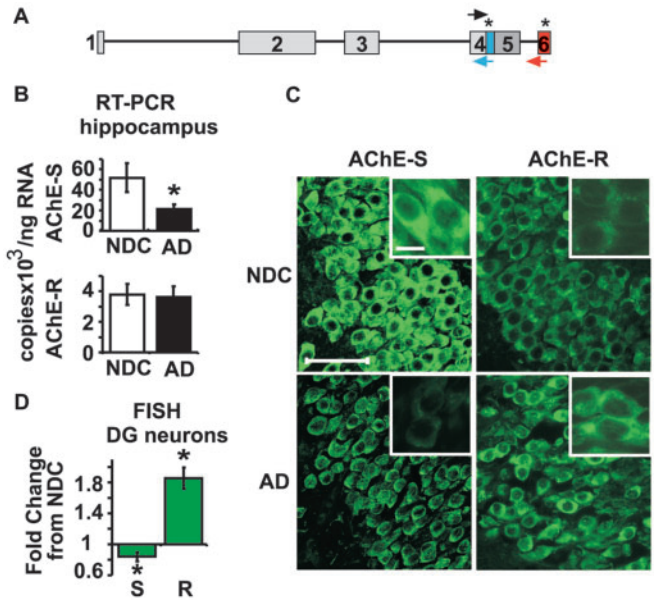

Fig. 5 Splice shift from AChE-S mRNA to AChE-R mRNA in hippocampal tissue of Alzheimer's disease patients. (**A**) Location of primers (arrows) and *in situ* hybridization probes (asterisks) used. (**B**) Real-time RT–PCR absolute quantification AChE splice variants from human hippocampal RNA. AChE-S mRNA levels are significantly reduced in Alzheimer's disease ($n = 10$) compared to non-demented control patients (NDC, $n = 5$). Copy number? 10^3/ng RNA ± SEM. ($^*P < 0.05$, Mann–Whitney test). (**C**) Fluorescent *in situ* hybridization (FISH) of human hippocampal sections using cRNA probes specific for each variant. Shown is the dentate gyrus (DG) area. Scale bar = 50 and 10 μm in micrographs and insets, respectively. (**D**) Fluorescent signal quantification shows decreased AChE-S and increased AChE-R mRNA levels in Alzheimer's disease DG compared to NDC neurons. Fold change from NDC ± SEM. ($^*P < 0.05$, Mann–Whitney test).

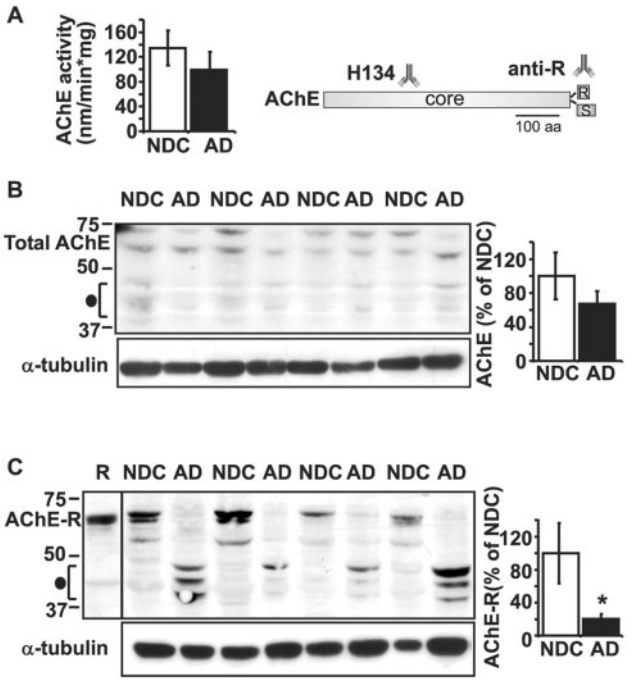

Fig. 6 AChE-R protein levels are reduced in the hippocampus of Alzheimer's disease patients. (**A**) Total AChE activity was measured in hippocampal homogenates from 10 Alzheimer's disease patients and five non-demented controls (NDC). (**B**) Total AChE immuno-blot of hippocampal homogenates from NDCs and Alzheimer's disease patients. A 30% decrease in labelling intensity of intact AChE is observed, similar to that seen in AChE activity. Note the presence of shorter degradation products (filled circle). Scheme: Total AChE was immuno-detected by an antibody that captures all AChE variants (HI34). (**C**) A specific antibody against AChE-R (anti-R) detected reduction to 20% of NDC levels in AChE-R protein levels from hippocampal homogenates of Alzheimer's disease patients ($^*P < 0.01$, Mann–Whitney test). R marks recombinant AChE-R positive control. α-tubulin labelling is shown as loading control in both (**B**) and (**C**). Note the Alzheimer's disease-associated increase in AChE-R degredation products (filled circle) migrating similarly to those labelled with the HI34 antibody.

Second, we measured AChE activity in hippocampal homogenates to determine the total hydrolytic activities of all AChE variants. An ~30% reduction was predictably found in AChE activity in our Alzheimer's disease samples compared to NDCs (Fig. 6A). Extraction of AChE-S enriched, LS detergent hippocampal fraction, confirmed that this reduction mainly results from reduced AChE-S levels. Thus, the activity of AChE-S was compatibly reduced by 20% in Alzheimer's disease samples. Immuno-blot analysis of hippocampal homogenates using polyclonal antibodies that capture all AChE variants (Fig. 6, scheme) further confirmed parallel reduction protein level, while demonstrating several faster migrating bands reflecting apparent proteolysis of hippocampal AChE (Fig. 6B). Importantly, an antibody selective for the AChE-R variant, revealed a drastic reduction of intact AChE-R levels, to about 20% of NDC levels (Fig. 6C, $P < 0.01$). Additionally, the anti-AChE-R antibody selectively detected substantially shortened AChE-R fragments in the hippocampus of Alzheimer's disease patients. Several of these fragments migrated similarly to those observed with the common antibody, suggesting that AChE-R in the Alzheimer's disease hippocampus is particularly susceptible to the disease-associated activation of proteases in the Alzheimer's disease brain (Saito *et al.*, 1993; Su *et al.*, 2001).Together, these results demonstrated increased neuronal AChE-R mRNA levels, which could potentially lead to overproduction of this neuroprotective protein by alternative splicing shift from the AChE-S form to AChE-R. However, protein analysis showed almost completely diminished AChE-R protein in the Alzheimer's disease brain, suggesting apparent malprotection.

Discussion

Alternative splicing serves to increase the repertoire of protein products from single genes (Maniatis and Tasic, 2002). Often, splice variants of specific genes play inverse roles in cell fate and function (Shin and Manley, 2004). Our current study demonstrates that this is the case also for

AChE splice variants, in the context of their inverse roles in Alzheimer's disease neuropathology. Compatible with previous findings, we found facilitated amyloid fibrils formation by AChE-S (Inestrosa *et al.*, 1996; Rees *et al.*, 2005). However, unlike AChE-S, we observed physiologically relevant and dose-dependent inhibition of Aβ fibrils formation by AChE-R *in vitro*, *ex vivo* and *in vivo*, in double-transgenic APPsw/AChE-R mice. Moreover, AChE-R limited the cellular toxicity of Aβ, reduced cortical astrocytes activation and protected dendritic integrity, all inverse to the capacity of AChE-S to increase the neurotoxic effect of Aβ (Alvarez *et al.*, 1998). Finally, we observed hippocampal loss of AChE-R in Alzheimer's disease patients, suggesting physiological relevance for Aβ neuropathology in the Alzheimer's disease brain. The two splice variants of AChE therefore exert multileveled inverse effects on both Aβ fibrils formation and neurotoxicity. Of note, the observed increase of AChE-R mRNA by *in situ* hybridization of hippocampal neurons and not by RT–PCR of the entire tissue suggests that this increase may only take place within neurons.

In mammals, AChE-R overexpression is induced by multiple stress stimuli as well as by aging (Meshorer and Soreq, 2006). Accordingly, we found an increase in the neuronal levels of AChE-R mRNA in Alzheimer's disease hippocampi, compatible with the stress and anxiety involved in Alzheimer's disease progression (Masugi *et al.*, 1989; Green *et al.*, 2006). In addition, neuronal increase of AChE-R mRNA may also result from a feedback mechanism following the degradation of the AChE-R protein and/or other Alzheimer's disease-related processes.

However, to fully exert its protective effects, AChE-R mRNA must yield the intact AChE-R protein. This does not occur in the Alzheimer's disease brain: unlike normal aging, the AChE-R protein is substantially downregulated in Alzheimer's disease, suggesting that an Alzheimer's disease-related process is responsible. It is note worthy that both AChE-R mRNA and the AChE-R protein are less stable than the corresponding AChE-S mRNA and AChE-S protein (Chan *et al.*, 1998; Cohen *et al.*, 2003). Therefore, alternative 3′ splicing of the AChE pre-mRNA transcript likely operates to increase the levels of the neuroprotective AChE-R but the protein product does not accumulate, likely due to exacerbated proteolysis. Interestingly, AChE fragments corresponding in size to those found in Alzheimer's disease hippocampal homogenates were also detected, albeit faintly, in NDCs by both anti-AChE and anti-AChE-R antibodies. However, a drastic increase in the immunoreactivity of these fragments was only detected by the anti-AChE-R antibody. Therefore, it appears that selective proteolysis of the AChE-R protein, which accounts for roughly 10% of total AChE, is induced in the Alzheimer's disease hippocampus. Moreover, it has been previously shown in a 1-year follow-up study (Darreh-Shori *et al.*, 2004) that untreated Alzheimer's disease patients exhibit a selective decline in AChE-R levels over time. Therefore, preliminary evidence suggests that the decline in AChE-R levels correlates with the disease progression. In the same study, rivastigmine administered for 1 year induced CSF AChE-R expression and a higher AChE-R/AChE-S ratio correlated with sustained cognition and improved behaviour in these Alzheimer's disease patients. Together, this supports the role of AChE-R as a neuroprotective agent. Interestingly, tacrine treatment resulted in a general upregulation of AChE, suggesting that AChE inhibitors exert different effects on the expression of specific AChE variants and that inhibitors which selectively increase AChE-R levels may be more potent drugs operating in a dual mode of action.

Amyloid fibrils formation involves generation of different intermediates with distinct toxic effects, which precede the formation of mature fibrils and aggregates (Ross and Poirier, 2004; Lesne *et al.*, 2006). Our cross-linking findings suggest that AChE-R interferes with the earliest stages of Aβ formation, providing the grounds for mechanistic explanation of the AChE-R-dependent reduction in Aβ toxicity. In these experiments, the AChE-R attenuation effect was limited in its duration. However, enforced increase of AChE-R by ~3-fold sufficed to reduce plaque burden in 75-week-old mice. This difference between the *in vitro* and *in vivo* outcome of AChE-R excess may be due to the distinct experimental conditions: *In vitro*, we used highly purified AChE-R and synthetic Aβ; *in vivo*, many other proteins could have affected fibrils formation.

AChE-S and AChE-R have identical enzymatic characteristics including K_m (0.33 ± 0.092, 0.29 ± 0.035 for AChE-R and AChE-S, respectively) and substrate inhibition (Farchi *et al.*, 2007). It is therefore expected that the different effects of AChE-S and AChE-R arise from non-enzymatic properties such as protein–protein interactions of their unique C-termini and/or their differential location in the synapse *in vivo* (membrane anchored and soluble, respectively).

Structural studies suggest that both AChE-S and AChE-R include the peripheral anionic site (PAS) reported to promote Aβ fibril formation (Alvarez *et al.*, 1998). However, they differ in their C-termini, suggesting that this region is responsible for the variant-specific effects on fibrils formation. For comparison, the AChE-homologous enzyme BChE, exerts a similarly effective attenuation of Aβ fibrils formation *via* its C-terminal domain, in a process involving an impaired amphipathicity due to a protruding aromatic tryptophan residue (Diamant *et al.*, 2006). AChE-R's C-terminus includes two tryptophan residues that may be functionally involved in Aβ fibril interactions (Wang and Hecht, 2002; Gazit, 2005). However, the C-terminal peptide of BChE likely resumes a helical structure, whereas the C-terminal peptide of AChE-R is a naturally unfolded peptide (Circular dichroism spectroscopy, data not shown). Further research will be required to determine the structure resumed by this naturally unfolded peptide when interacting with Aβ.

That overexpression of AChE-R protects neurons from both aging (Sternfeld *et al.*, 2000) and Aβ-induced neuropathologies, and that it elevates hippocampal long-term potentiation (Nijholt *et al.*, 2004) supports the notion that the selective loss of AChE-R has a pivotal role in the Aβ-induced toxicity in AD. Thus the ability of AChE-R to protect against aging-dependent neurodeterioration also in mice lacking amyloid pathology further suggests that AChE-R can protect neurons by additional mechanism(s) apart from delaying Aβ fibrils formation. Compatible with this hypothesis, AChE-R excess also protects dopaminergic neurons from MPTP neurotoxicity (Ben-Shaul *et al.*, 2006). Therefore, AChE-R loss may contribute by itself to neuronal toxicity in Alzheimer's disease. Failure to overproduce AChE-R at need is also likely to impair cognitive stress reactions (Meshorer and Soreq, 2006). Supporting this suggestion, transgenic downregulation of AChE-R results in failure to terminate neuronal stress reactions accompanied by impaired dendritic formation (Sklan *et al.*, 2006).

Taken together, our findings reveal a novel linkage between the cholinergic system and amyloid pathology while changing the common understanding of AChE's involvement in Alzheimer's disease. The inverse *in vitro*, *ex vivo* and *in vivo* effects of the AChE-S and AChE-R splice variants on amyloid fibril formation, further suggest alternative splicing-induced differences as the underlying mechanism for these distinct effects. Our findings of a neuroprotective effect of AChE-R may further foreshadow a putative future therapeutic treatment involving the AChE-R protein.

Acknowledgements

The funding was provided by The German Israel Project DIP-G 3.2, European Community's Network of Excellence (LSH-2004-1.1.5-3) and STREP (LSHG-CT 2006-037277), the Hebrew University's Eric Roland Center for Neurodegenerative Diseases and the Interdisciplinary Center for Neuronal Computation (ICNC), to H.S; The Defense Advance Research Project Agency (#N66001-01-C-8015) to T.S.M and H.S. The authors wish to thank Dr Naomi Melamed-Book for confocal microscopy assistance and Mr Erez Podoloy for structural advice.

References

Alvarez A, Alarcon R, Opazo C, Campos EO, Munoz FJ, Calderon FH, et al. Stable complexes involving acetylcholinesterase and amyloid-beta peptide change the biochemical properties of the enzyme and increase the neurotoxicity of Alzheimer's fibrils. J Neurosci 1998; 18: 3213–23.

Ben-Shaul Y, Benmoyal-Segal L, Ben-Ari S, Bergman H, Soreq H. Adaptive acetylcholinesterase splicing patterns attenuate 1-methyl-4-phenyl-1,2,3,6-tetrahydropyridine-induced Parkinsonism in mice. Eur J Neurosci 2006; 23: 2915–22.

Ben Aziz-Aloya R, Seidman S, Timberg R, Sternfeld M, Zakut H, Soreq H. Expression of a human acetylcholinesterase promoter-reporter construct in developing neuromuscular junctions of Xenopus embryos. Proc Natl Acad Sci USA 1993; 90: 2471–5.

Braak H, Braak E. Neuropathological stageing of Alzheimer-related changes. Acta Neuropathol (Berl.) 1991; 82: 239–59.

Caccamo A, Oddo S, Billings LM, Green KN, Martinez-Coria H, Fisher A, et al. M1 receptors play a central role in modulating AD-like pathology in transgenic mice. Neuron 2006; 49: 671–82.

Carson KA, Geula C, Mesulam MM. Electron microscopic localization of cholinesterase activity in Alzheimer brain tissue. Brain Res 1991; 540: 204–8.

Chan RY, Adatia FA, Krupa AM, Jasmin BJ. Increased expression of acetylcholinesterase T and R transcripts during hematopoietic differentiation is accompanied by parallel elevations in the levels of their respective molecular forms. J Biol Chem 1998; 273: 9727–33.

Cohen O, Reichenberg A, Perry C, Ginzberg D, Pollmacher T, Soreq H, et al. Endotoxin-induced changes in human working and declarative memory associate with cleavage of plasma ''readthrough'' acetylcholinesterase. J Mol Neurosci 2003; 21: 199–212.

Coyle JT, Price DL, DeLong MR. Alzheimer's disease: a disorder of cortical cholinergic innervation. Science 1983; 219: 1184–90.

Cummings JL, Back C. The cholinergic hypothesis of neuropsychiatric symptoms in Alzheimer's disease. Am J Geriatr Psychiatry 1998; 6: S64–78.

Darreh-Shori T, Hellstrom-Lindahl E, Flores-Flores C, Guan ZZ, Soreq H, Nordberg A. Long-lasting acetylcholinesterase splice variations in anticholinesterase-treated Alzheimer's disease patients. J Neurochem 2004; 88: 1102–13.

Davis KL, Mohs RC, Marin D, Purohit DP, Perl DP, Lantz M, et al. Cholinergic markers in elderly patients with early signs of Alzheimer disease. JAMA 1999; 281: 1401–6.

Diamant S, Azem A, Weiss C, Goloubinoff P. Increased efficiency of GroE-assisted protein folding by manganese ions. J Biol Chem 1995; 270: 28387–91.

Diamant S, Podoly E, Friedler A, Ligumsky H, Livnah O, Soreq H. Butyrylcholinesterase attenuates amyloid fibril formation in vitro. Proc Natl Acad Sci USA 2006; 103: 8628–33.

Ellman GL, Courtney KD, Andres V, Jr, Feather-Stone RM. A new and rapid colorimetric determination of acetylcholinesterase activity. Biochem Pharmacol 1961; 7: 88–95.

Evron T, Geyer BC, Cherni I, Muralidharan M, Kilbourne J, Fletcher SP, et al. Plant-derived human acetylcholinesterase-R provides protection from lethal organophosphate poisoning and its chronic aftermath. FASEB J 2007; 21: 2961–9.

Fancy DA, Kodadek T. Chemistry for the analysis of protein-protein interactions: rapid and efficient cross-linking triggered by long wavelength light. Proc Natl Acad Sci USA 1999; 96: 6020–4.

Farchi N, Ofek K, Podoly E, Dong H, Xiang YY, Diamant S, et al. Peripheral site acetylcholinesterase blockade induces RACK1-associated neuronal remodeling. Neurodegener Dis 2007; 4: 171–84.

Gazit E. Mechanisms of amyloid fibril self-assembly and inhibition. Model short peptides as a key research tool. FEBS J 2005; 272: 5971–8.

Geyer BC, Muralidharan M, Cherni I, Doran J, Fletcher SP, Evron T, et al. Purification of transgenic plant-derived recombinant human acetylcholinesterase-R. Chem Biol Interact 2005; 157–158: 331–4.

Gilboa-Geffen A, Lacoste PP, Soreq L, Cizeron-Clairac G, Le Panse R, Truffault F, et al. The thymic theme of acetylcholinesterase splice variants in Myasthenia gravis. Blood 2007; 109: 4383–91.

Green KN, Billings LM, Roozendaal B, McGaugh JL, LaFerla FM. Glucocorticoids increase amyloid-beta and tau pathology in a mouse model of Alzheimer's disease. J Neurosci 2006; 26: 9047–56.

Hsiao K, Chapman P, Nilsen S, Eckman C, Harigaya Y, Younkin S, et al. Correlative memory deficits, Abeta elevation, and amyloid plaques in transgenic mice. Science 1996; 274: 99–102.

Inestrosa NC, Alvarez A, Perez CA, Moreno RD, Vicente M, Linker C, et al. Acetylcholinesterase accelerates assembly of amyloid-beta-peptides into Alzheimer's fibrils: possible role of the peripheral site of the enzyme. Neuron 1996; 16: 881–91.

Kaufer D, Friedman A, Seidman S, Soreq H. Acute stress facilitates long-lasting changes in cholinergic gene expression. Nature 1998; 393: 373–7.

Klug GM, Losic D, Subasinghe SS, Aguilar MI, Martin LL, Small DH. Beta-amyloid protein oligomers induced by metal ions and acid pH are distinct from those generated by slow spontaneous ageing at neutral pH. Eur J Biochem 2003; 270: 4282–93.

Landwehrmeyer B, Probst A, Palacios JM, Mengod G. Expression of acetylcholinesterase messenger RNA in human brain: an in situ hybridization study. Neuroscience 1993; 57: 615–34.

Lesne S, Koh MT, Kotilinek L, Kayed R, Glabe CG, Yang A, et al. A specific amyloid-beta protein assembly in the brain impairs memory. Nature 2006; 440: 352–7.

LeVine H, III. Thioflavine T interaction with synthetic Alzheimer's disease beta-amyloid peptides: detection of amyloid aggregation in solution. Protein Sci 1993; 2: 404–10.

Lleo A, Greenberg SM, Growdon JH. Current pharmacotherapy for Alzheimer's disease. Annu Rev Med 2006; 57: 513–33.

Maniatis T, Tasic B. Alternative pre-mRNA splicing and proteome expansion in metazoans. Nature 2002; 418: 236–43.

Massoulie J. The origin of the molecular diversity and functional anchoring of cholinesterases. Neurosignals 2002; 11: 130–43.

Masugi F, Ogihara T, Sakaguchi K, Otsuka A, Tsuchiya Y, Morimoto S, et al. High plasma levels of cortisol in patients with senile dementia of the Alzheimer's type. Methods Find Exp Clin Pharmacol 1989; 11: 707–10.

Matsuoka Y, Picciano M, Malester B, LaFrancois J, Zehr C, Daeschner JM, et al. Inflammatory responses to amyloidosis in a transgenic mouse model of Alzheimer's disease. Am J Pathol 2001; 158: 1345–54.

Meshorer E, Soreq H. Virtues and woes of AChE alternative splicing in stress-related neuropathologies. Trends Neurosci 2006; 29: 216–24.

Nijholt I, Farchi N, Kye M, Sklan EH, Shoham S, Verbeure B, et al. Stress-induced alternative splicing of acetylcholinesterase results in enhanced fear memory and long-term potentiation. Mol Psychiatry 2004; 9: 174–83.

Pick M, Perry C, Lapidot T, Guimaraes-Sternberg C, Naparstek E, Deutsch V, et al. Stress-induced cholinergic signaling promotes inflammation-associated thrombopoiesis. Blood 2006; 107: 3397–406.

Rees TM, Berson A, Sklan EH, Younkin L, Younkin S, Brimijoin S, et al. Memory deficits correlating with acetylcholinesterase splice shift and amyloid burden in doubly transgenic mice. Curr Alzheimer Res 2005; 2: 291–300.

Ross CA, Poirier MA. Protein aggregation and neurodegenerative disease. Nat Med 2004; 10 (Suppl): S10–7.

Saito K, Elce JS, Hamos JE, Nixon RA. Widespread activation of calcium-activated neutral proteinase (calpain) in the brain in Alzheimer disease: a potential molecular basis for neuronal degeneration. Proc Natl Acad Sci USA 1993; 90: 2628–32.

Shin C, Manley JL. Cell signalling and the control of pre-mRNA splicing. Nat Rev Mol Cell Biol 2004; 5: 727–38.

Sklan EH, Berson A, Birikh KR, Gutnick A, Shahar O, Shoham S, et al. Acetylcholinesterase modulates stress-induced motor responses through catalytic and noncatalytic properties. Biol Psychiatry 2006; 60: 741–51.

Sklan EH, Lowenthal A, Korner M, Ritov Y, Landers DM, Rankinen T, et al. Acetylcholinesterase/paraoxonase genotype and expression predict anxiety scores in Health, Risk Factors, Exercise Training, and Genetics study. Proc Natl Acad Sci USA 2004; 101: 5512–7.

Soreq H, Ben-Aziz R, Prody CA, Seidman S, Gnatt A, Neville L, et al. Molecular cloning and construction of the coding region for human acetylcholinesterase reveals a G + C-rich attenuating structure. Proc Natl Acad Sci USA 1990; 87: 9688–92.

Sternfeld M, Shoham S, Klein O, Flores-Flores C, Evron T, Idelson GH, et al. Excess ''read-through'' acetylcholinesterase attenuates but the ''synaptic'' variant intensifies neurodeterioration correlates. Proc Natl Acad Sci USA 2000; 97: 8647–52.

Su JH, Zhao M, Anderson AJ, Srinivasan A, Cotman CW. Activated caspase-3 expression in Alzheimer's and aged control brain: correlation with Alzheimer pathology. Brain Res 2001; 898: 350–7.

Sun A, Nguyen XV, Bing G. Comparative analysis of an improved thioflavin-s stain, Gallyas silver stain, and immunohistochemistry for neurofibrillary tangle demonstration on the same sections. J Histochem Cytochem 2002; 50: 463–72.

Tsai J, Grutzendler J, Duff K, Gan WB. Fibrillar amyloid deposition leads to local synaptic abnormalities and breakage of neuronal branches. Nat Neurosci 2004; 7: 1181–3.

Wang W, Hecht MH. Rationally designed mutations convert de novo amyloid-like fibrils into monomeric beta-sheet proteins. Proc Natl Acad Sci USA 2002; 99: 2760–5.